Construction of a Spin-Echo Small-Angle Neutron Scattering Instrument for the PIK Reactor

Chetverikov, Yu O.; Akselrod, L. A.; Grigor'ev, S. V.; Kraan, V.; Sumbatyan, A. A.; Nagorny, A. V.; Tarnavich, V. V.

DOI
10.1134/S1027451022050287

Publication date
2022

Document Version
Final published version

Published in
Journal of Surface Investigation

ISSN 1027-4510, Journal of Surface Investigation: X-ray, Synchrotron and Neutron Techniques, 2022, Vol. 16, No. 5, pp. 831–838. © Pleiades Publishing, Ltd., 2022.
Russian Text © The Author(s), 2022, published in Poverkhnost', 2022, No. 10, pp. 16–23.

Construction of a Spin-Echo Small-Angle Neutron Scattering Instrument for the PIK Reactor

Yu. O. Chetverikov[a, *], L. A. Akselrod[a], S. V. Grigor'ev[a], V. Kraan[b], A. A. Sumbatyan[a], A. V. Nagorny[c, d, e], and V. V. Tarnavich[a]

[a] *Konstantinov Petersburg Nuclear Physics Institute, National Research Center "Kurchatov Institute," Gatchina, 188300 Russia*

[b] *Delft Technical University, 2600 AA, Delft, The Netherlands*

[c] *Joint Institute for Nuclear Research, Dubna, 141980 Russia*

[d] *Taras Shevchenko National University of Kyiv, Kyiv, 03022 Ukraine*

[e] *Institute of Environmental Geochemistry of the National Academy of Sciences of Ukraine, Kyiv, 02000 Ukraine*

**e-mail: chetverikov_yo@pnpi.nrcki.ru*

Received January 14, 2022; revised March 25, 2022; accepted March 25, 2022

Abstract—The current state of the implementation of the project for building a spin-echo instrument for small-angle neutron scattering at the PIK reactor of the St. Petersburg Nuclear Physics Institute, National Research Center "Kurchatov Institute," is described. In the course of the project, work is carried out on mathematical modeling, and the design and manufacture of prototypes of the instrument units. Both the optical elements of the instrument and the design of the precession magnets are optimized. The developed model of precession magnets underlies the design submitted for manufacturing. The model of a radio-frequency adiabatic flipper is tested. The test results demonstrate the flipper performance in the range of fields with an induction from 5 to 66 mT.

Keywords: small-angle neutron scattering, neutron spin echo, submicron structure of matter

DOI: 10.1134/S1027451022050287

INTRODUCTION

The spin-echo small-angle neutron scattering (SESANS) method [1] significantly expands the possibilities of traditional methods of small-angle and ultra-small-angle scattering. Due to the high luminosity of SESANS instruments, when studying the structure of matter at scales from 100 nm to 40 μm, the measurement time is reduced by several times.

Using the SESANS method, many experimental problems have been solved, both for studying materials in a wide range of structural scales from several nanometers to several microns (fractal objects, chromatin packing in the nucleus of a biological cell) [2–5], and for increasing the efficiency of measurements of ultra-small-angle scattering by objects with large-scale (more than 100 nm) inhomogeneities (magnetic domains, photonic crystals, colloidal solutions) [6–8].

OPERATING PRINCIPLE AND CHARACTERISTICS OF THE PIK-REACTOR SESANS INSTRUMENT

The operation of the SESANS instrument is as follows. Neutrons produced and thermalized in a reactor are fed through a neutron-guide system to the instrument. The neutron pulse is generated by a double-disk chopper and is detected in the time channels specified by the chopper start signal. Polarizing mirrors transmit neutrons with one spin state (along the magnetic field of the polarizer) and absorb neutrons with another state. The precession of polarized neutrons begins with a polarization rotator, which rotates the magnetic moment of the neutron by $\pi/2$ with respect to the leading field ($\pi/2$ rotator). The operation of the precession fields of the SESANS instrument is illustrated in Fig. 1. The neutron trajectory passes through the first and second magnets of the first precession arm. In the magnetic field of the first precession arm, each neutron acquires its own unique phase, which depends both on the wavelength (energy) of the neutron and on the trajectory in the magnetic field. The direction of the field in the second arm is reversed.

A sign change occurs on the current screen, which is located at the boundary between the arms and produces a magnetic field with such an abrupt transition that the neutron polarization does not follow the field (is not an adiabatic transition). In the second arm of the instrument, identical to the first one, precession is carried out in the opposite direction.

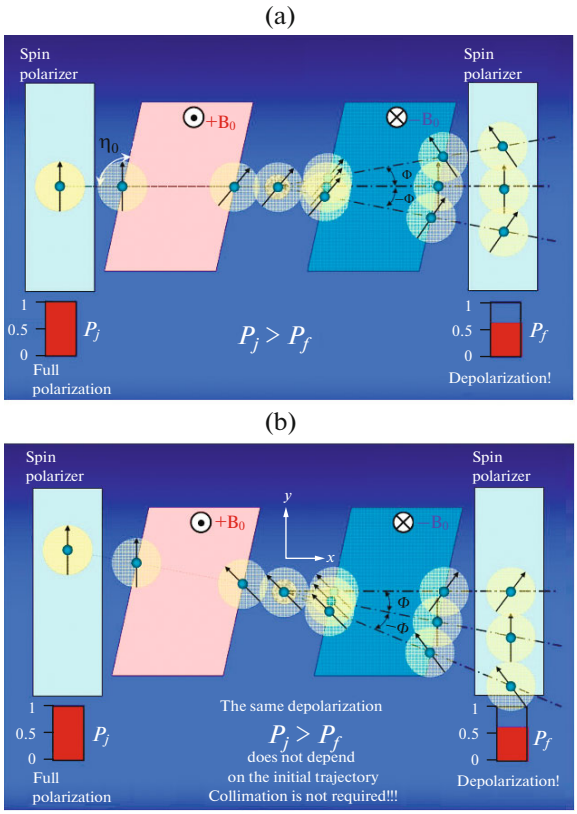

Fig. 1. Scheme of SESANS measurements: a change in the neutron trajectory due to scattering at the sample leads to depolarization of the neutron beam; b depolarization is almost independent of the neutron-beam collimation.

If there is no scattering sample at the center of the instrument, then, propagating in the second arm along a trajectory similar to that in the first arm, the neutron acquires the same precession phase as in the first arm. At the end of the second arm, a $\pi/2$ rotator is mounted, after which the polarization coincides with the initial one, and the precession stops.

A change in the neutron trajectory due to scattering at the sample leads to the fact that the trajectories and phases of precession in the first and second arms of the instrument become nonequivalent, and the phase inhomogeneity of the neutron beam is manifested in depolarization. In order for the spin-echo signal to be as sensitive as possible to small scattering angles at the sample, the configuration of the magnetic field of the instrument is such that the field boundary is located at an acute angle to the incident neutron beam.

The tuning parameters jointly affect the value of the depolarization and can be summarized by the Fourier transform parameter of the transmitted scattering pulse, i.e., the "spin-echo length" [1]:

$$\delta = \frac{m\gamma_n BL\lambda^2 \mathrm{ctan}\theta_0}{2\pi h}, \qquad (1)$$

where m and γ_n are the mass and gyromagnetic ratio of the neutron, respectively; B is the magnetic-field induction of the precession magnet; L is the length of the magnetic-field region along the beam; λ is the neutron wavelength; θ_0 is the tilt angle of the magnet-field boundary with respect to the incident beam; h is Planck's constant. The change in polarization, determined by the set of precession phases of scattered and nonscattered neutrons, is expressed as follows [1]:

$$P'(\delta) = \frac{P_\delta}{P_0} = (1-s) + s\langle P_{SC}(\delta)\rangle, \qquad (2)$$

P_0 is the polarization of the beam passed without scattering, s is the total scattering cross section, $1-s$ is the fraction of nonscattered neutrons, $\langle P_{SC}(\delta)\rangle$ is the average polarization of scattered neutrons:

$$\langle P_{SC}(\delta)\rangle = \frac{1}{sk_0^2}\int_{-\infty}^{\infty} S(\mathbf{Q})\cos(zQ_\delta)\,d^2Q, \qquad (3)$$

$S(Q)d^2Q$ is the fraction of neutrons scattered in the range of wave vectors $d^2Q = dQ_y dQ_z$ (y is the horizontal direction, perpendicular to the beam axis; z is the vertical direction).

The dependence $P_{SC}(\delta)$ measured by the spin-echo method contains the Fourier transform of the scattering projection $S_\delta(\mathbf{Q})$, which is uniquely determined by the scattering function of the sample $S(\mathbf{Q})$. The Fourier transform $S_\delta(\mathbf{Q})$ transforms the scattering process from reciprocal space into direct space, and for elastic scattering (a process without a change in the neutron energy during scattering) we obtain:

$$G_{SE}(\delta) = \frac{1}{4^2}\int_V^0\int_{-\infty}^{\infty}\int_{-\infty}^{\infty} G(\mathbf{R})\exp(-i(\mathbf{QR} - Q_\delta\delta))d\mathbf{R}dQ_y dQ_z, \qquad (4)$$

where $G_{SE}(\delta)$ is the correlation function, which is the reduced polarization of the neutron beam $\langle P_{SC}(\delta)\rangle$, scattered by the sample. Here the cosine is replaced by a complex exponent, and as a result of two-way integration, the complex part represented by sine disappears. After integration over Q_Z, z, Q_y and y and taking $Q_x = 0$, we obtain:

$$G_{SE}(\delta) = \int_{-\infty}^{\infty} G(x,0,z)\,dx. \qquad (5)$$

It can be seen that such a representation of $G_{SE}(\delta)$ corresponds to the projection of the sample correlation function $G(\mathbf{R})$ onto the z direction.

The spin-echo technique for studying small-angle neutron scattering, in contrast to the traditional technique (recording scattering from a small angular deviation of a part of a well-collimated neutron beam), uses the principles of neutron spin echo to encode the scattering angle in a way that is independent of the primary-beam collimation. Thus, the feedback between

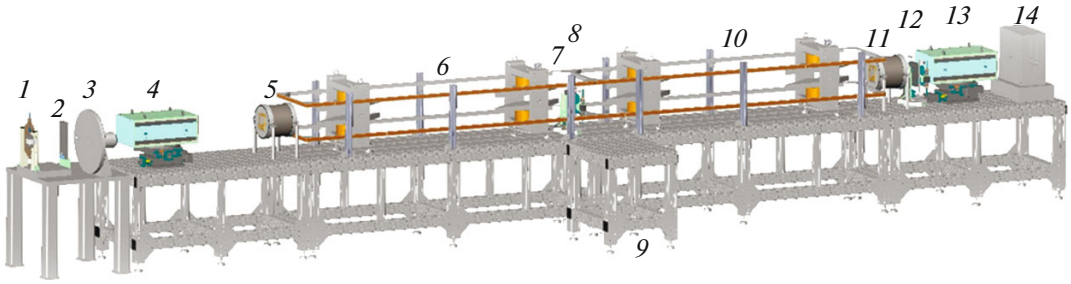

Fig. 2. Scheme of the SESANS PIK instrument: (*1*) monitor with a diaphragm; (*2*) damper; (*3*) chopper; (*4*) polarizer; (*5*) first $\pi/2$ rotator; (*6*) first arm of precession; (*7*) diaphragm of the sample; (*8*) current screen; (*9*) sample table; (*10*) second precession arm; (*11*) second $\pi/2$ rotator; (*12*) analyzer diaphragm; (*13*) analyzer; (*14*) detector.

the intensity of incident neutrons and the resolution of the instrument breaks down. In practice, this means that it is possible to measure the scattering of a sample at ultra-small angles in a beam whose angular divergence exceeds by orders of magnitude the range of scattering angles under study.

The PIK SESANS instrument has a field configuration with radio frequency (RF) flippers. The spatial splitting of neutron waves in this configuration occurs due to the absorption or emission of a virtual energy quantum by a radio-frequency field of coils tuned in resonance with the Larmor precession of the neutron spin.

In general terms, a description of the operation of the arm of a resonance spin-echo instrument is given in [9]. The δ value from Eq. (1) can be described as the distance between two quantum states of a neutron wave (with spin along and against the field) after splitting at a tilted field boundary. Entering the radio-frequency flipper, the split waves exchange energy with the radio-frequency field of the flipper so that the energy quantum is exactly equal to the Zeeman energy difference between the two spin states of a neutron in a constant magnetic field:

$$\hbar\omega_{RF} = -2\mu_n B, \qquad (6)$$

moreover, the amplitude of the radio frequency field B_{RF} is chosen in such a way that the probability of a spin flip is $\rho = 1$. The velocities of neutron waves after passing through the flipper do not change, but only their spin states change. After passing through the flipper, the waves continue to diverge at the same velocity as before the flipper. At the second boundary of the field, inverted neutron waves again change their velocity. The difference in the velocities of the inverted waves increase by $2\Delta k$, therefore, after the field, the waves continue to scatter at an even higher rate. Entering the second arm magnet, parts of the neutron wave again change their velocity, so that the difference in the velocities of waves with different spins decreases. Having passed through the second flipper, which, like the first one, exchange the energy of the radio-frequency field with the neutron, neutron waves, without changing their velocity, change the spin states. When leaving the second field, refraction occurs, as a result of which the velocities of neutron waves become equal, and spatial separation stops.

The spatial separation of neutron waves corresponds to the "spin-echo length" given for the "classical" (nonresonant) spin echo by Eq. (1). In the case of a resonance spin echo, the "zero-field precession" phase is determined not so much by the length of the magnets as by the distance between them. Therefore, for a resonance spin echo, there is no need to create an extended field of magnets. Resonance spin echo can be conveniently implemented in facilities with time-of-flight measurements, when the pulse contains neutrons of a wide spectral range. In this case, an adiabatic RF flipper [10] with a powerful RF field generator [11] is used.

The SESANS instrument is planned to be placed at the H3-2 neutron guide of building 104 of the PIK-reactor complex. Figure 2 shows the general scheme of the instrument. In the figure, the neutron beam sequentially passes from the first diaphragm to the detector through the instrument from left to right. The main SESANS parameters for the PIK-reactor complex are given in Table 1.

MAGNETIC SYSTEM

The magnetic system of the instrument (Fig. 3) consists of electromagnets of the precession field with radio-frequency adiabatic flippers located in them, polarization rotators, leading field coils, and a current screen.

A vertical field with an induction from zero to 0.1 T is created in the interpolar space of the magnet. The pole pieces of the magnet are shaped like a parallelogram with an acute angle of 33.5°. The magnets are arranged so that the beam axis passes through the center of the magnet at the same acute angle to the field boundary. The magnets are located in pairs in each arm at a distance of about 1.5 m. An adiabatic radio-frequency flipper with coils of gradient and radio-frequency fields is placed in the interpolar gap of each magnet. A gradient field (also vertical) with an amplitude of about 5–10 G is created by currents in a special

Table 1. Physical parameters of the SESANS PIK instrument

Wavelength range, nm	0.35–1.2
Wavelength resolution $d\lambda/\lambda$	0.1
Range of measured scales	100 nm–40 μm
Range of magnetic fields of the main magnets, T	0–0.1
Scanning mode	Time-of-flight mode; variation of the field of the main magnets
Frequency range of variable fields of the flippers, MHz	0.15–3
Instrument length, m	8
Polarizing efficiency of the polarizer and analyzer	≥0.95
Maximum cross section of the neutron beam on the sample, mm^2	10 × 10
Scattering plane	Horizontal
Detector	Finger 3He

system of conductors. To create a radio-frequency field (amplitude 10–15 G), a rectangular solenoid with an axis coinciding with the beam axis is used. The solenoid is connected to a RF current generator, which provides currents with an amplitude of about 6 A in the range from 50 kHz to 3 MHz [12].

The adiabatic π/2 polarization rotator ensures rotation of the polarization vector by 90° with respect to the leading field. The rotator is a combination of six windings placed in a magnetic screen providing various options for the smooth transition of fields from one coordinate axis to another with a non-adiabatic boundary between the fields. Windings providing fields in the plane perpendicular to the beam are V shaped and made of aluminum wires (to reduce neutron absorption).

The leading magnetic field (on the order of 1 mT) is created by a pair of rectangular coils with dimensions of 30 × 500 × 2500 mm located above and below the beam at a distance of about 400 mm from each other. The field created by such coils is sufficiently uniform over the beam cross section. In the arms of the instrument, the leading fields are oppositely directed.

The current screen (field stepper) is located at the center of the instrument. This device is necessary for the formation of a sharp (nonadiabatic) magnetic boundary during the transition from the first to the second arm. The current screen is a foil with direct current. The maximum induction of the field created by the device is 0.7–1 mT, the field gradient when crossing the boundary is about 14 mT/cm.

OPTICAL SCHEME OF THE INSTRUMENT

The optical scheme of the instrument is shown in Fig. 4 and consists of a disk chopper, a polarizer, an

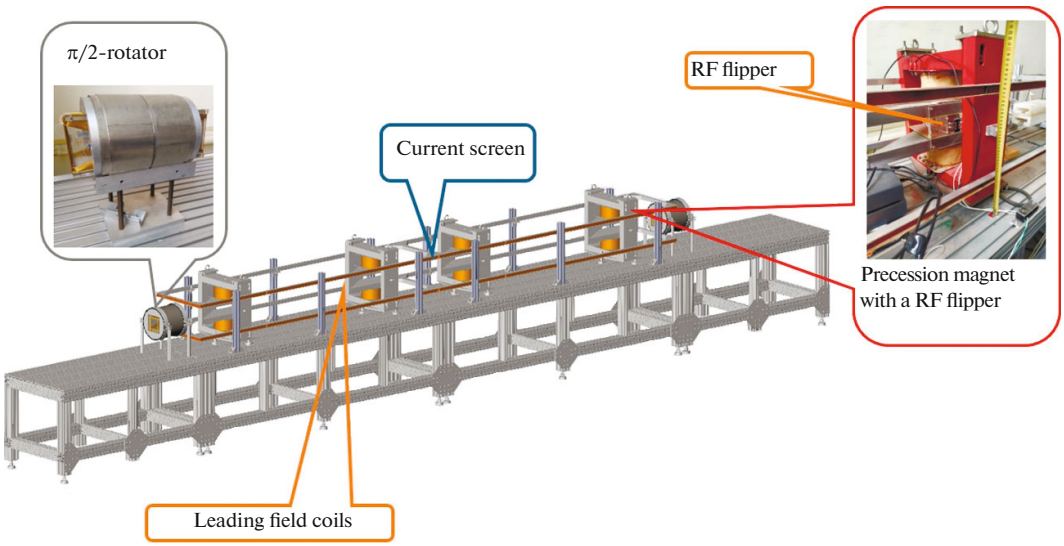

Fig. 3. Magnetic system of the SESANS PIK instrument.

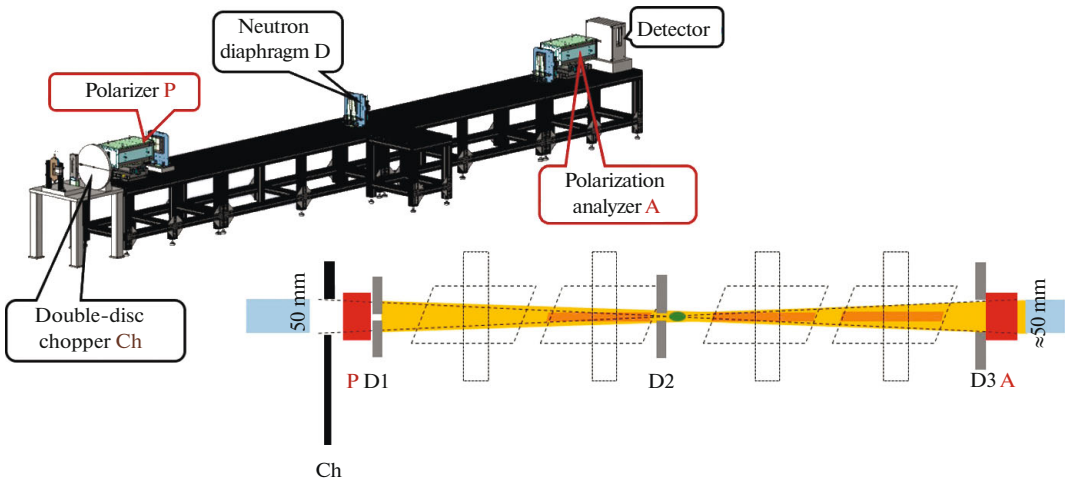

Fig. 4. SESANS optical scheme.

analyzer, and three sets of collimating diaphragms (D1–D3). The size of the input window of the diaphragm D1 near the polarizer (8 × 50 mm) is limited by the size of the working area of the field of the main magnets. The diaphragm D2 near the sample cuts out a beam from the neutron flux with a cross section of 8 × 10 mm. The dimensions of the diaphragm window are determined by the maximum cross section of the samples under study. The size of diaphragm D3 near the analyzer of 8 × 50 mm is determined by the minimum measurable scale (limited to 100 nm due to large angle scattering and diagram shutter absorption). The beam converging in the horizontal plane from 50-mm diaphragm D1 to 10-mm diaphragm D2 is potentially capable of increasing the neutron flux by a factor of five compared to a parallel beam (10-mm D1 and 10-mm D2) and implements the possibility of measuring small-angle scattering in a diverging neutron beam.

The disk chopper is designed to form a neutron pulse, provide time-of-flight measurements and is optimized for operation in the wavelength range of 3–12 Å with a resolution of $\Delta\lambda/\lambda \sim 10\%$. The chopper consists of two disks rigidly fixed on the same axis. The chopper axis is located on the side of the neutron-guide axis and parallel to it. The distance between the discs is 1 m. The radius of the discs is 250 mm. Each disk is made of neutron-absorbing material and has two through windows. The disks are deployed so that the windows of the first disk are covered by the second disk, forming an "optically blind" scheme. A double-disk chopper, in contrast to a single-disk chopper, is characterized by an almost constant resolution $d\lambda/\lambda$ over the entire measured wavelength range λ and a relatively high transmission at large λ. A useful feature of such a scheme is reduction of the direct radiation background of ionizing radiation from the reactor. The chopper displacement unit, in case of need for measurements in the case of a direct beam, allows the chopper to be completely removed from the beam.

As a polarizing element of both the polarizer and the analyzer, a V-shaped supermirror optical assembly (V cavity) is used: two flat mirrors 385 mm long, located in the form of the letter V with an angle at the apex of ~0.9° (two critical reflection angles). The beam axis passes along the central assembly line at an angle of 0.45° to each mirror. The mirror connection line is located horizontally across the beam axis, as is the magnetic field (on the order of 50 mT) created by a system of permanent magnets located around the polarizer and setting the direction of polarization. Polarizing supermirrors are multilayer Fe/Si coatings deposited onto both sides of a single-crystal plate (0.3 mm thick) with the reflectivity $m = 5$. The positively polarized component is reflected from the mirrors and leaves the beam, while the negatively polarized component passes through the mirror and is used in the instrument (mirror size of 50 × 385 mm). The magnet with the optical assembly is located on the adjustment table with two degrees of freedom: it is possible to move it horizontally across the beam and rotate it about the vertical axis. The input cross sections of both the polarizer and analyzer are 10 × 50 mm.

Radiation shield around the chopper and polarizer ensures the absorption of radiation that occurs during modulation of the neutron beam (absorption of neutrons in the discs of the chopper, reflection of neutrons by the polarizer mirror) to acceptable levels.

Diaphragms (D1–D3) are designed to shape the beam size horizontally and vertically using movable shutters with a neutron-absorbing coating and automated adjustment of the distance between the shutters. Horizontal and vertical shutters synchronously change their position relative to the central position. To ensure the possibility of combining the axis of the device with the axis of the beam, automated horizontal

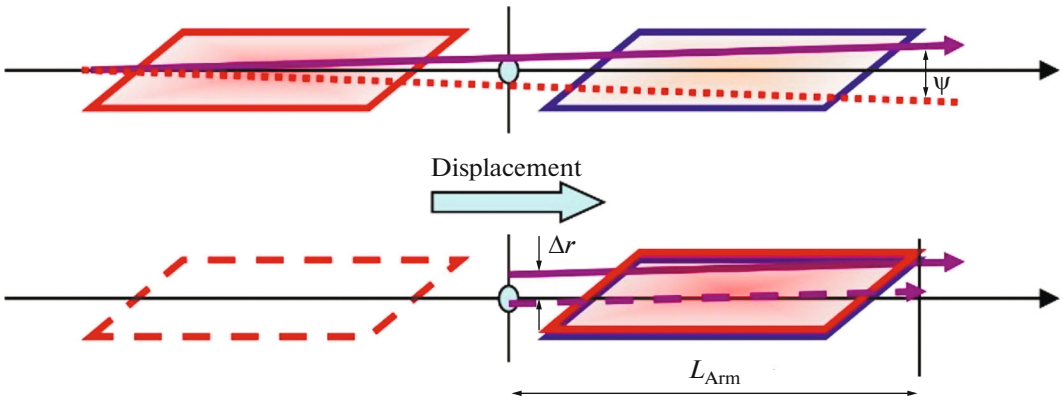

Fig. 5. Comparison of trajectories in the two arms of the device. Any trajectories that are not parallel to the axis of the device do not coincide, and the phases in the first and second arms for them are not equal to each other.

translators are used that move the diaphragm unit across the neutron beam.

The sample unit varies depending on the task but includes the following basic parts: a linear translator of movement in the range of 200 mm across the beam for automated sample displacement, a table with vertical movement in the range of 50 mm for placement of the cryostat or oven; the allowable load is 50 kg. All parts made of magnetic materials are as far away from the beam as possible to eliminate the effect of polarization on the wiring.

CURRENT STATUS OF THE INSTRUMENT-CONSTRUCTION PROJECT

To improve the efficiency of the SESANS instrument under construction at the PIK reactor, work has been carried out to improve the performance of the precession magnet and the adiabatic resonance flipper. The efficiency of the instrument can be estimated based on the savings in measurement time. The required measurement time is found from the dispersion of the useful signal [13] (the scatter of experimental points around the values located on the G_{SE} scattering curve), which decreases with the set of statistics:

$$D(G_{SE}) = \frac{1 + (s(G_{SE} - 1) + 1)^2 \left(1 - 2P_0^2\right)}{tI_{SE}s^2P_0^2}, \qquad (7)$$

where t and I_{SE} are the measurement time and the intensity on the sample. The quantity $D_1(G_{SE})$ is strongly affected by the degree of polarization P_0. This effect is most pronounced for a small fraction of scattered neutrons (s).

The magnetic-field induction B and precession-region length L determine the precession phase as

$$j \sim \Sigma B_{x,y,z} dL/dx, \qquad (8)$$

where $B_{x,y,z}$ is the field induction at a trajectory point with the coordinates x, y, and z (summation is performed over the entire trajectory from the beginning to the end of the precession area), and the quantity $\sum B_{x,y,z} dL/dx$ is the field integral (BL) of the magnets along the neutron flight path. During spin-echo measurements, the instrument is adjusted so that the phase in the first arm of the instrument φ_I is equal to the phase in the second arm φ_{II}, which leads to zero phase difference after the second arm: $\varphi_{I-II} = \varphi_I - \varphi_{II} = 0$. Then the polarization at the output of the device P_f is equal to the polarization at the input to the device P_i. However, due to the inhomogeneity of the field over the beam cross section, for trajectories not parallel to the instrument axis, the condition $\varphi_{I-II} = 0$ is not fulfilled. The origin of the phase φ_{I-II} is shown in Fig. 5. The spin-echo instrument can be presented as a system with translational symmetry. If the translation operation is performed, then the arms I and II are combined with each other. It can be seen that the deviation of the neutron from the instrument axis by the angle ψ leads to a discrepancy between the trajectories of the first and second arms and the distance between the trajectories Δr. In the case of the field inhomogeneity inside the magnet ($B_{x,y,z} \neq \langle B \rangle$) the depolarization ($P_f < P_i$) arises, which worsens the quality of measurements. Increasing the homogeneity of the field integral of the precession magnets makes it possible to improve the polarization P_f and thus reduce the measurement time.

During construction of the instrument, the work was done to simulate the magnet and optimize the homogeneity of the field integral. As a result of the work done, a magnet (Fig. 6) with improved magnetic characteristics was developed (Table 2). The production process of the developed electromagnet was launched.

In the configuration of the SESANS instrument with adiabatic RF flippers, the P_0 value is also critically affected by the spin-flip probability ρ in the flippers. Since the adiabatic flipper operates in each of the four magnets, $P_0 \sim f(\rho)^4$.

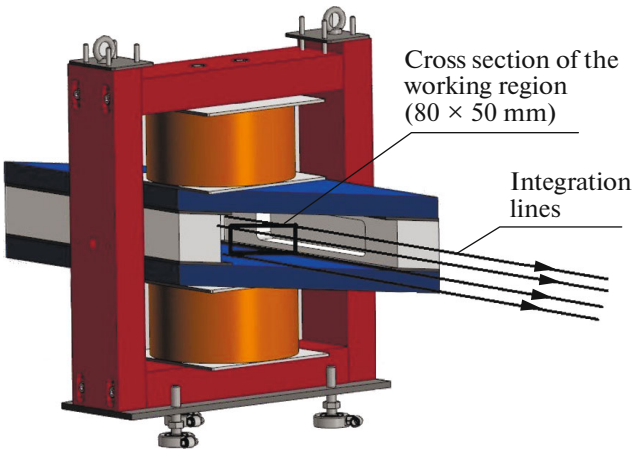

Fig. 6. Sketch of the electromagnet of the SESANS PIK instrument.

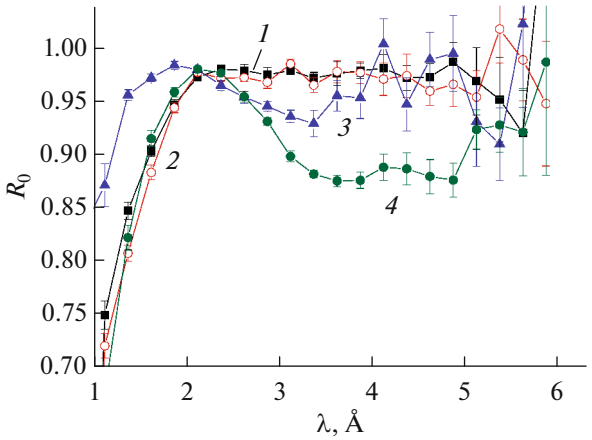

Fig. 7. Dependence of the flipper spin-flip probability on the neutron wavelength: (*1*) f = 150 kHz, B = 4.9 mT; (*2*)–f = 365 kHz, B = 12 mT; (*3*) f = 1 MHz, B = 33.1 mT; (*4*) –f = 2 MHz, B = 66 mT.

The flipper design was tested at the REFLEX neutron station of the IBR-2 research reactor (Dubna). Figure 7 shows the dependence of the spin-flip probability ρ on the neutron wavelength. It can be seen that with increasing wavelength from 1 to 2.2 Å, the spin-flip efficiency reaches a maximum value of 0.975 for all four measured frequencies (fields) of the flipper tuning. At frequencies of 150 and 365 kHz, in the λ range from 2.2 to 6, the spin-flip probability remains maximum, varying only within the statistical deviation of the measurements, while in the case of high frequencies of 1 and 2 MHz, the spin-flip efficiency decreases at λ > 2.2 Å. At a frequency of 1 MHz, the minimum efficiency of 0.93 corresponds to λ = 3.4 Å, at 2 MHz, a wide minimum of 0.88 extends from λ = 3.5 to 5 Å.

The experiment showed that despite the revealed high efficiency of the spin flip of 0.975 (at the tuning point λ = 2.2 Å) in the frequency range (fields of the precession magnet) from 150 to 365 kHz, the observed decrease in the spin-flip efficiency to 0.9 in the long-wavelength part of the spectrum at frequencies of 1 and 2 MHz significantly reduces the overall efficiency of the SESANS instrument. Based on the results of experimental work, a number of changes have been made to the design of the flippers. Testing of the new design is scheduled for the end of October 2022.

CONCLUSIONS

As of the end of September 2021, the entire complex of research and development work on the creation of the SESANS device has been completed. Most of the working design documentation has been developed. Work on optimizing the design of the RF adiabatic flipper is planned to be completed at the end of October 2022. The procurement of materials and equipment is underway. The assembly of units of the instrument is planned to be completed by the fall of 2022, and the instrument is to be installed by December 2022.

Table 2. Characteristics of the electromagnet of the SESANS instrument for the PIK reactor

Magnetic-field induction at the center of the air gap, T	0–0.1
Air gap (pole distance), mm	90
Field integral BL, T m	0.066 ± 0.004
Working region W × H, mm × mm	50 × 8
Homogeneity of the field integral $\Delta BL/BL$ (x, y) in the working region, T m	$\leq 2.5 \times 10^{-4}$
Magnet width, mm	≤570
Magnet height, mm	≤740
Magnetic-field direction	Vertical
Weight of electromagnet, kg	≤500
Tilt angle of the equal field lines with respect to the integration lines, deg	33.5

FUNDING

The work on prototyping and certification of the RF adiabatic flipper design was supported by the Russian Science Foundation (project no. 19-12-00363).

CONFLICT OF INTEREST

We declare that we have no conflicts of interest.

REFERENCES

1. M. T. Rekveldt, J. Plomp, W. G. Bouwman, W. H. Kraan, S. Grigoriev, and M. Blaauw, Rev. Sci. Instrum. **76**, 033901 (2005).
2. E. G. Iashina, M. V. Filatov, R. A. Pantina, E. Y. Varfolomeeva, W. G. Bouwman, C. P. Duif, D. Hondecker, V. Popich, and S. V. Grigoriev, J. Appl. Crystallogr. **52**, 844 (2019).
3. E. G. Iashina, E. V. Velichko, M. V. Filatov, W. G. Bouwman, C. P. Duif, A. Brulet, and S. V. Grigoriev, Phys. Rev. E **96**, 012411 (2017).
4. E. G. Iashina, W. G. Bouwman, C. P. Duif, M. V. Filatov, and S. V. Grigoriev, J. Phys.: Conf. Ser. **862**, 012010 (2017).
5. E. V. Velichko, A. L. Buyanov, N. N. Saprykina, Y. O. Chetverikov, C. P. Duif, W. G. Bouwman, and R. Y. Smyslov, Eur. Polym. J. **88**, 269 (2017).
6. E. V. Velichko, Y. O. Chetverikov, L. A. Aksel'rod, V. N. Zabenkin, V. V. Piyadov, A. A. Sumbatyan, W. H. Kraan, and S. V. Grigor'ev, J. Surf. Invest.: X-ray, Synchrotron Neutron Tech. **7**, 401 (2013).
7. S. V. Grigoriev, Y. O. Chetverikov, V. N. Zabenkin, W. H. Kraan, M. T. Rekveldt, and N. van Dijk, J. Appl. Crystallogr. **40**, s111 (2007).
8. W. H. Kraan, V. N. Zabenkin, Y. A. Chetveriko, M. T. Rekveldt, C. P. Duif, and S. V. Grigoriev, Phys. B (Amsterdam, Neth.) **397**, 79 (2007).
9. W. H. Kraan, L. A. Akselrod, E. G. Yashina, A. A. Sumbatyan, and S. V. Grigoriev, J. Sur. Invest.: X-ray, Synchrotron Neutron Tech. **14**, S108 (2020).
10. S. V. Grigoriev, R. Kreuger, W. H. Kraan, F. M. Mulder, and M. T. Rekveldt, Phys. Rev. A: **64**, 013614 (2001).
11. A. N. Bazhenov, V. M. Lobashev, A. N. Pirozhkov, and V. N. Slusar, Nucl. Instrum. Methods Phys. Res., Sect. A **332**, 535 (1993).
12. A. A. Sumbatyan, RF Patent No. 2017100229; Byull. Izobret., No. 19 (2017).
13. Yu. O. Chetverikov, Candidate's Dissertation in Mathematics and Physics (Petersburg Inst. Nucl. Phys., St. Petersburg, 2011).

Translated by L. Mosina